Role of Tool Shoulder Diameter in Friction Stir Welding: An Analysis of the Temperature and Plastic Deformation of AA 2014 Aluminium Alloy

K. Ramanjaneyulu · G. Madhusudhan Reddy ·
A. Venugopal Rao

Abstract The influence of tool shoulder diameter and its rotational speed on the high temperature plastic deformation of the material during friction stir welding of AA 2014 aluminum alloy is investigated, using the principles of hot working. The soundness of weld and defect formation are analyzed using the Zener–Hollomon parameter 'Z' to describe the high temperature plastic deformation behaviour of material, under the simultaneous influence of temperature and strain-rate. The observed hot deformation behaviour is correlated with the deformation processing map for the first time. At a given rotational speed, the volume of shoulder driven flow reduces with increasing shoulder diameter.

1 Introduction

The welding of aluminum and its alloys has always posed serious challenges to designers and technologists. Several difficulties such as porosity, hot cracking and distortion are associated with the fusion welding of aluminum alloys [1, 2]. These problems can be controlled to a large extent by employing solid-state welding processes. Friction stir welding (FSW) process is an emerging solid-state joining process in which the material that is being welded does not melt and recast [2, 3]. The advantages of FSW over conventional fusion welding have been reported by many researchers, particularly for the industries that rely heavily on joining of aluminum alloys [2, 3]. The significant advantages in the fabrication of aluminium structures using FSW are the elimination of weldment cracking and porosity, apart from obviating the need for filler metal and expensive weld joint preparation. However, to realize its potential fully, the weld formation mechanisms associated with FSW must be clearly understood. In recent years, a significant progress has been made in understanding the physical processes that occur during the welding of aluminum alloys. Nevertheless, many aspects of the process are still poorly understood and require further study, e.g. temperature field in the nugget and thermo-mechanically affected zones (TMAZ).

Tool geometry is the significant factor that controls the material flow and heat generation in FSW. The key feature of the FSW tool geometry are (i) shoulder, responsible for the generation of frictional heat during the process and facilitating material movement around the pin and (ii) pin, whose primary function is to deform the material around it and its secondary function, is to generate heat. In order to control material flow, heat generation and maximize the welding speed, several tool designs have been evolved with different features [4]. However, a unified approach to FSW tool design, based on sound scientific principles, is seldom reported in published literature [5].

The individual influence of FSW tool shoulder and pin configurations, on the quality of aluminum alloy joints has often been studied separately. Extensive studies have also been carried out on the role of pin geometry in deformation and heat generation, during the FSW of aluminum alloys [6–13]. The pin is reported to contribute to the heat

K. Ramanjaneyulu
Mahatma Gandhi Institute of Technology, Hyderabad, India

G. Madhusudhan Reddy (✉) · A. Venugopal Rao
Defence Metallurgical Research Laboratory, Hyderabad, India
e-mail: gmreddy_dmrl@yahoo.co.in; msreddy@dmrl.drdo.in

generation through plastic deformation, thereby complimenting the frictional heat generation at the shoulder. The influence of shoulder diameter on frictional heat generation and consequent plastic deformation, ultimately resulting in the weld joint formation, has been studied from different perspectives [14–20]. The tool shoulder causes adequate softening and facilitates plastic flow of the workpiece material at relatively lower power and torque levels, thereby enhancing the tool life. Elangovan and Balasubramanian [11] studied the influence of tool shoulder diameter on the mechanical properties, observing that only one of the three diameters resulted in superior weld tensile properties during the FSW of AA 6061. The reasons for this behaviour are neither thoroughly understood nor did the study provide any guidelines for the design of tool geometry. Arora et al. [18] proposed a criterion for the design of shoulder diameter based on the principle of maximum utilization of supplied (input) torque for traction. The criterion identifies the optimum shoulder diameter as one that causes equal partitioning of the supplied torque between sticking and sliding. The optimization of shoulder diameter also depends on the rotational speed (rpm) of the tool. Subsequently, Mehta et al. [21] correlated the experimentally measured temperatures and torque with the results from this criterion. An understanding of the influence of shoulder diameter on peak temperature, torque and spindle power requirements for all tool rotational speeds was considered. It was concluded that, as the shoulder diameter increases, the state of the deforming material changes from high flow-stress and low temperature to low flow-stress and high temperature. Zhang et al. [22] studied the influence of shoulder diameter on weld temperature and material deformation using finite element method (FEM). An increase in the shoulder diameter resulted in an increase in the peak temperatures with the temperature distribution becoming relatively uniform with increasing shoulder diameter (underneath the shoulder). Titilayo and Akinwale [23] reported an increase in advancing force, downward vertical force and torque with increasing shoulder diameters. These findings were reported at a constant tool tilt angle to minimize the occurrence of weld defects. The depth of penetration and tool tilt were kept constant irrespective of the shoulder diameter used. The pin configuration, however, remained unchanged for all tools. This obviously results in a decrease in the actual area of the shoulder being in contact with the workpiece (in all the cases less than half of the shoulder area). Additionally, maintaining a constant shoulder penetration results in an effective reduction in the pin penetration into the workpiece. This incomplete pin penetration in turn results in an imperfect joint, apart from causing an inadequate exploitation of the advantages due to larger shoulder diameter employed. Thus, the influence of shoulder diameter on

FSW vis-à-vis the tool tilt angle is not explicitly understood. With regard to the influence of tool on the FSW flow field, two different modes of tool related flows are frequently mentioned in literature: shoulder driven flow and pin driven flow [12, 14, 24–28]. Although several studies concerning the influence of pin geometry on material flow during FSW have been carried out [25, 29, 30], the influence of shoulder geometry on material flow is still unexplored. The present paper aims to bridge these gaps, with an attempt to develop an understanding of the physics of the process.

2 Experimental Procedure

Friction stir welding of 5 mm thick aluminum alloy AA 2014-T6 in square butt joint configuration, was carried out on FSW machine (ETA Make). The FSW tools were prepared from H-13 tool steel with a conical tool pin profile with threads. The shoulder diameter of the tool was varied from 11.5 to 24 mm (2.3–4.8 times the plate thickness, respectively) and the details of the fabricated tools are shown in Fig. 1. The pin profile (conical with thread) was kept constant for all tools, thereby ensuring that the shoulder diameter is the only variation from tool to tool. Several experiments were carried out by varying tool rotational speed from 600 to 2,400 rpm at an increment of 200 rpm, but maintaining a constant traverse speed of 600 mm/min. Based on the appearance of weld bead surfaces, it was adjudged that, welds fabricated at 1,000 rpm with different shoulder diameters were found to be acceptable. Hence, in the subsequent experiments, the tool rotational speed was maintained constant at 1,000 rpm while varying the tool shoulder diameter. Other welding parameters employed in this investigation are presented in Table 1. During welding, temperatures were measured using a GRAPHTECH data-logger (Model-GL900) with K-type thermocouples, at the rate of 20 acquisitions per second. The thermocouples were inserted at a distance of 3 mm from the weld centerline and 2 mm below the top surface of the plate, on the advancing side of the weld (where the direction of the tool rotation is same as the direction of the tool travel). Transient temperatures for the entire duration of FSW were captured at three different locations on the advancing side. A schematic diagram of location of the thermocouples is presented in Fig. 2. The heat input was estimated for each shoulder diameter using the equation [23].

$$Q = \eta \frac{2\pi\omega T}{\vartheta}, \tag{1}$$

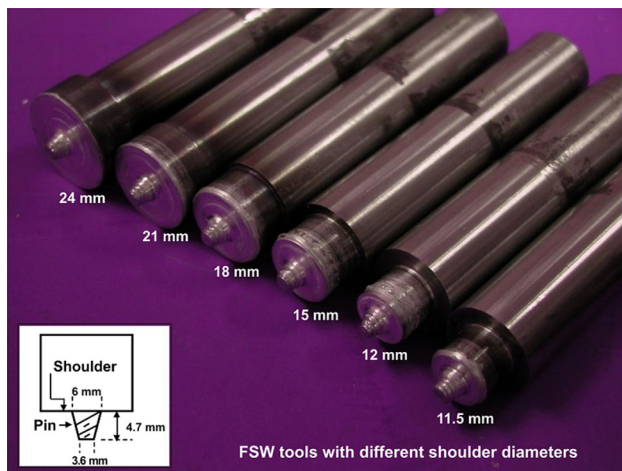where Q = heat input (J/mm), η = efficiency factor = 0.9 for Al, ω = rotational speed (rpm), T = torque (N m) and

Fig. 1 FSW tools with different shoulder diameters

Table 1 Parameters used during friction stir welding

Friction stir welding parameters	Units
Spindle speed	1,000 rpm
Traverse speed	600 mm/min
Tilt angle	2°
Dwell time	3 s

ϑ = feed rate (mm/min). All the weldments were sectioned perpendicular to the weld direction and the samples were prepared as per standard metallographic techniques for microstructural analysis. The electron back-scattered diffraction (EBSD) measurements were carried out using scanning electron microscope (SEM) equipped with EBSD system (TexSEM Laboratory, make). The EBSD was operated at an accelerating voltage of 20 kV and the measurements were obtained at a step size of 0–1.0 μm. Line-intercept method was employed for the measurement of grain size. Differential scanning calorimetry (DSC) was carried out for the welds produced by each of the shoulder diameters and base metal for comparison, by extracting 10 mg of metal from the stirred zone. The extracted metal/sample was subjected to a heating rate of 10 °C/min, from the ambient temperature (35 °C) to 550 °C, to estimate the fraction of precipitates dissolved during FSW. A schematic of the FSW process together with the coordinate system of forces is shown in Fig. 3. The data regarding spindle torque (N m), Z-axis force (kN) and X-axis force (kN) acting on the pin was acquired from online data acquisition system of the machine.

FSW is a high temperature deformation process where the flow-stress is critical to determine the high temperature plasticity of the metal [31]. Since flow-stress is a function of temperature and strain-rate at hot working temperatures, it is essential to factor in simultaneously the effect of both parameters. This is especially necessary because of the
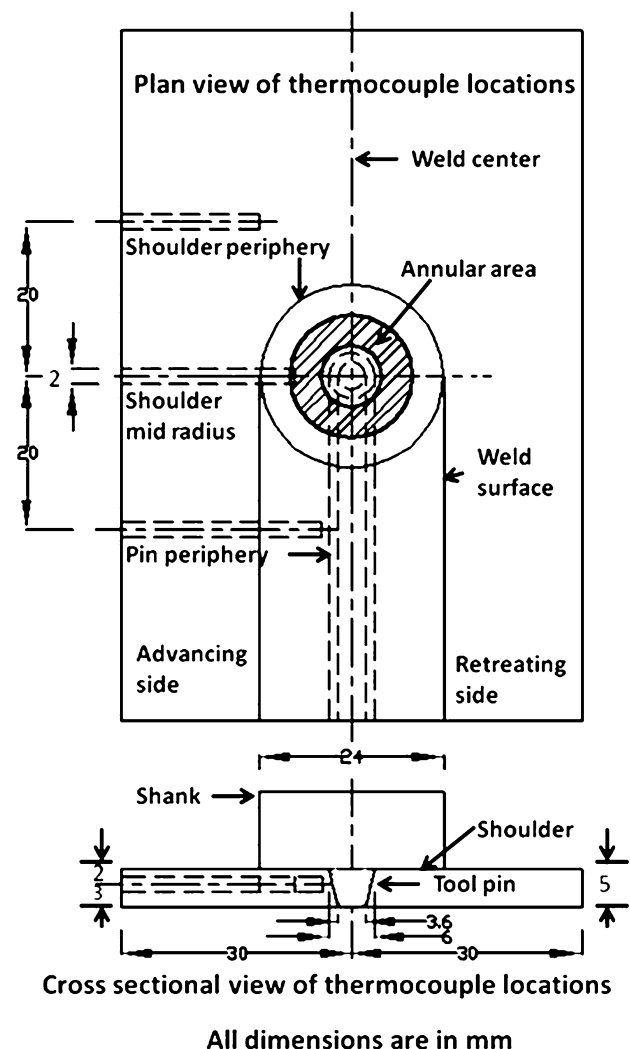

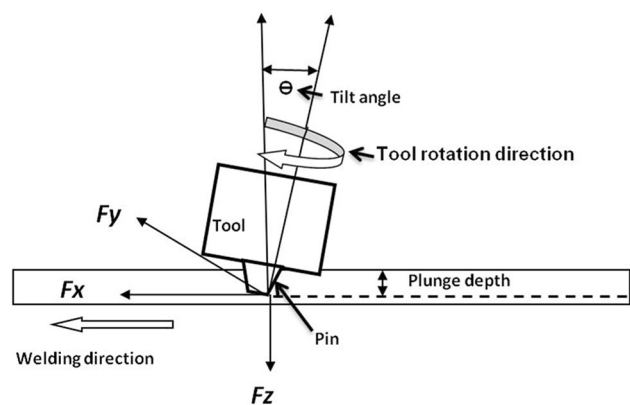Fig. 2 A schematic diagram of location of thermocouples

Fig. 3 A schematic diagram of FSW process and coordinate system of forces

high strain-rate encountered in FSW. The temperature compensated strain-rate, frequently referred to as the Zener–Hollomon parameter 'Z', best describes the ability

of the material for plastic deformation and thereby the soundness of the weld joint in FSW. Since the high temperature flow-stress is a function of 'Z', it may be considered as an index of the level of plasticity of the material in FSW. The Zener–Hollomon parameter is given by.

$$Z = \dot{\varepsilon} \exp\left(\frac{Q}{RT}\right), \tag{2}$$

where $\dot{\varepsilon}$ is strain-rate (per sec), Q is activation energy, 145 kJ/mol for the aluminum alloy [17, 32], R is universal gas constant, 8.314 J/mol/K, and T is temperature in K. For evaluation of 'Z', the temperature and strain-rate are the vital inputs from the experiments. Natural-strain or true-strain (ε) was estimated by using the equation [33–36].

$$\varepsilon = \ln\left(\frac{l}{APR}\right) + \left|\ln\left(\frac{APR}{l}\right)\right|, \tag{3}$$

where APR is the tool advance per revolution and l is deformed length and is expressed as
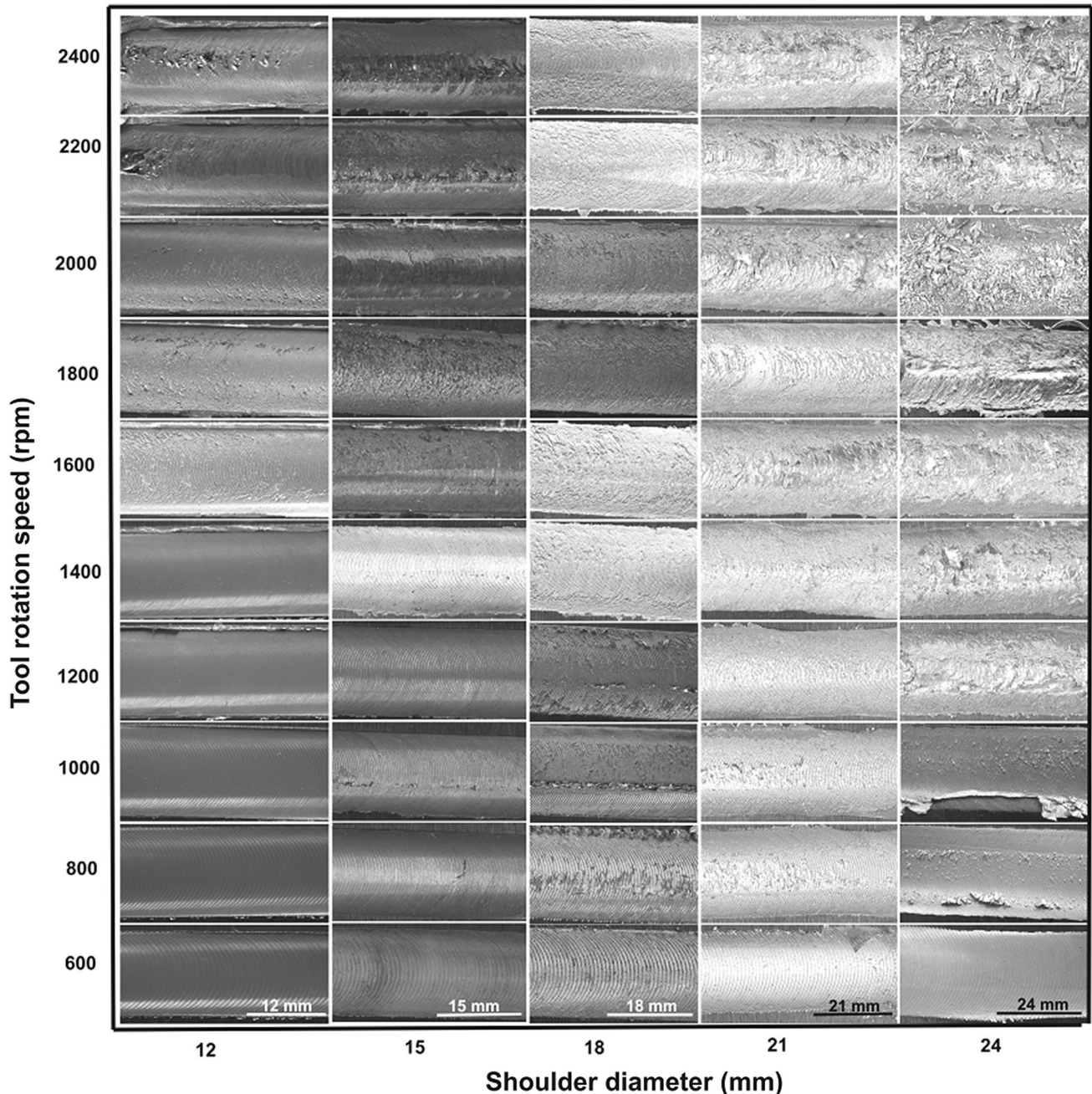

Fig. 4 Appearance of weld surfaces for various shoulder diameters with different tool rotational speeds

$$l = 2r\cos^{-1}\left(\frac{r-x}{r}\right), \tag{4}$$

where r is the probe diameter (mm) and x is the distance (mm), perpendicular to the welding direction, from the retreating side of the tool to the streamline in question. Since a tapered tool was used in this study to process the material, an arithmetic average of pin radius at root and tool tip was used in the calculation of strain. The strain-rate ($\dot{\varepsilon}$) was estimated using the equation

$$\dot{\varepsilon} = \frac{\varepsilon}{t}, \tag{5}$$

where 't' is time in seconds and is calculated by dividing APR by travel speed 'ϑ'. For evaluation of 'Z' outside the weld nugget region, experimentally measured temperatures were used. For estimation of 'Z' in the nugget region, the temperatures were evaluated (due to severe plastic deformation in the weld nugget, it was not possible to measure the temperature using contact method such as thermocouple) using the equation [37],

$$\frac{T}{T_m} = K\left(\frac{\omega^2}{\vartheta \times 10^4}\right)^\alpha, \tag{6}$$

where T, is peak temperature (°C), and T_m, is melting point (°C) of the material being processed. K, and α are constants ranging from 0.65 to 0.75 and 0.04 to 0.06, respectively. ω is tool rotational speed (rpm) and 'ϑ' is travel speed (in./min). In the current calculation, K equal to 0.75 and α equal to 0.06 were chosen to get the peak temperature during FSW. The estimated temperature from Eq. 6 is used for evaluation of 'Z' in the nugget zone.

3 Results and Discussion

3.1 Appearance of Weld Surfaces

The appearance of the weld bead surfaces was found to be varying with shoulder diameter variation and the tool rotational speed, for each of the shoulder diameters (Fig. 4). At relatively lower shoulder diameters, the weld

beads were defect-free for most part of the range of tool rotational speeds. Surface defects in the stir zone were found to be occurring at very high rotational speeds (viz. 2,000–2,400 rpm). This may be attributed to inadequate plasticity, caused by insufficient frictional heat generated by the shoulder. For larger shoulder diameters (18–24 mm), the surface defects appeared even at low rotational speeds. It may be observed from the Table 2 that the ratio of heat generating annular area to the shoulder area decreases with increase in shoulder diameter. Beyond the shoulder diameter of 15 mm, this ratio reduces to a minimum and remains almost constant thereafter. This trend indicates saturation in the frictional heat generation, inspite of the increase in the physical size of the shoulder. That is, a larger shoulder rotates over a region whose plasticity has reached a maximum threshold. Thus, at larger shoulder diameters, surface defects appear even at lower rotational speeds.

The appearance of weld bead surfaces produced (at tool rotation speed 1,000 rpm and traverse speed of 600 mm/min) with different shoulder diameters is presented in Fig. 5. It may be noted that at the minimum shoulder diameter of 11.5 mm, there are surface defects induced by inadequate plasticity in the stirred zone. The weld bead appearance is smooth without any surface defects in the welds produced with shoulder diameters of 12 and 15 mm. With a further increase in shoulder diameters from 18 to 24 mm, surface defects of a different kind indicating excessive heating were observed. These defects may be attributed to variations in heat generation and plastic deformation, in turn influenced by the tool shoulder diameter.

3.2 Temperature and Forces

It is believed that in FSW of thin sheets, most heat is generated by the shoulder therefore shoulder diameter can affect heat generation and peak temperatures of the materials during FSW [38–41]. Variation of peak temperatures below the shoulder, at the Nugget/TMAZ interface, is shown in Fig. 6. Spatial temperature gradient under the

Table 2 Ratio of annular area to shoulder area

Sl. no.	Shoulder diameter (mm)	Shoulder radius(r) = D/2 R (mm)	a = r/3 (mm)	b = 2r/3 (mm)	Annular area $\pi(b^2 - a^2)$ mm^2 (A)	Shoulder area (mm^2) $S_A = \pi r^2$	Pin area (mm^2) $P_A = \pi r^2$	$S_A - P_A$ mm^2 (B)	Ratio of A and B (A/B)
1	11.5	5.75	1.91	3.83	34.63	103.86	28.27	75.59	0.4581
2	12	6	2	4	37.69	113.09	28.27	84.82	0.4444
3	15	7.5	2.5	5	58.90	176.71	28.27	147.94	0.3981
4	18	9	3	6	84.82	254.47	28.27	225.68	0.3758
5	21	10.5	3.5	7	115.45	346.36	28.27	317.58	0.3635
6	24	12	4	8	150.8	452.39	28.27	424.10	0.3559
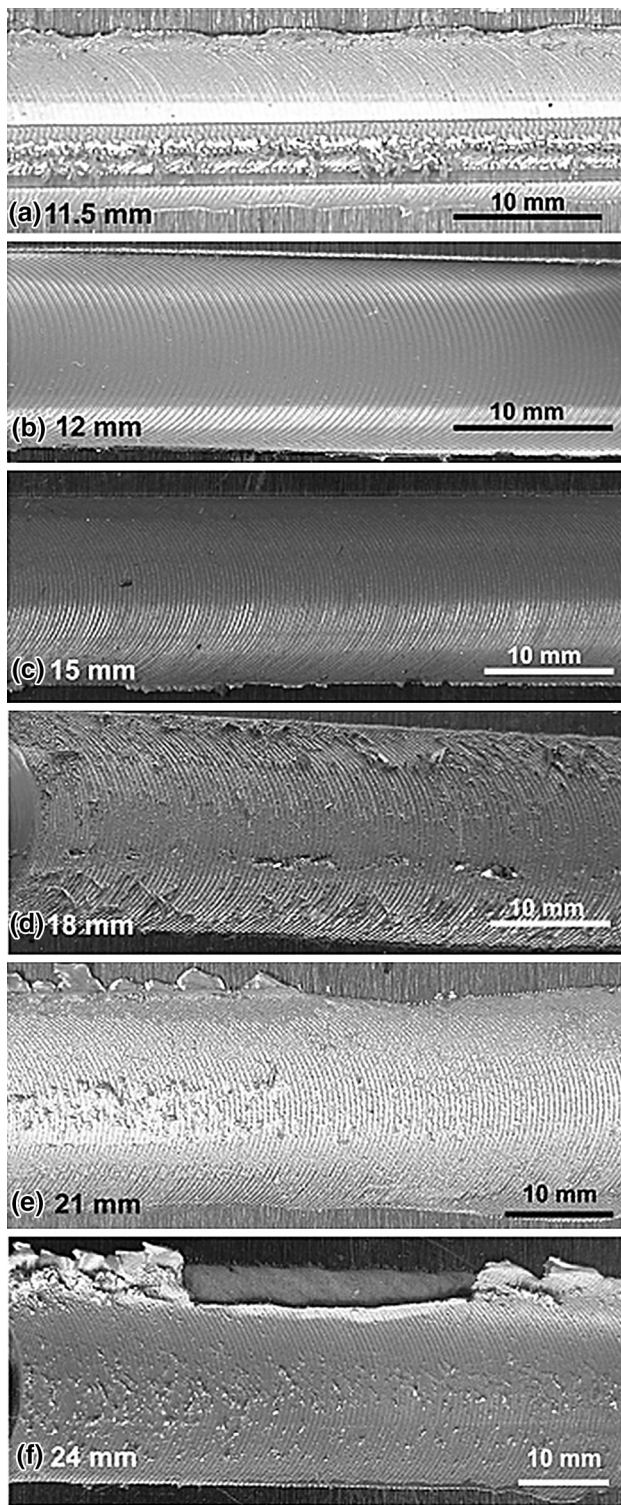
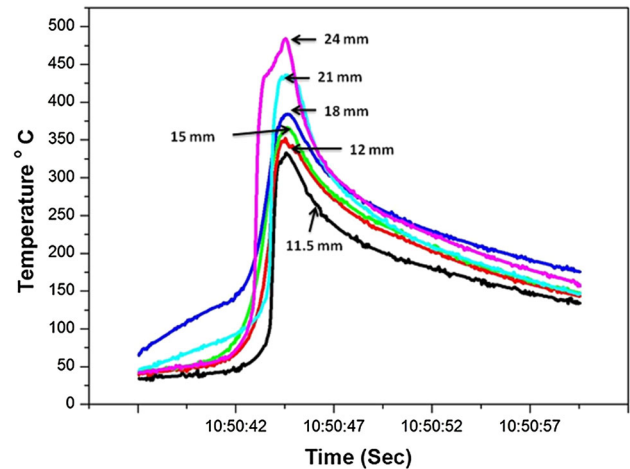Fig. 5 Weld surfaces produced by different shoulder diameters at 1,000 rpm

Fig. 6 Variation of peak temperatures below the shoulder of various diameters

Beyond this, there is a moderate decrease in the gradient up to 24 mm shoulder diameter. Heat input was plotted against each of the shoulder diameters, for the welding parameters investigated, as shown in Fig. 7. Increasing the shoulder diameter leads to an increase in the heat input and peak temperatures, due to an increase in frictional area.

The effect of the shoulder diameter could also be observed on the measured X-axis force, Z-axis force and torque. A representative example of force and torque profiles for the welds produced by the 12 mm shoulder diameter after steady state is shown in Fig. 8. X-axis force represents the force exerted by the plate on the tool against its translation direction, while z-axis force and torque act along and about the tool axis, respectively. Variation of torque and force with shoulder diameter is shown in Fig. 9. The vertical downward force (Z-axis force) and spindle torque increase monotonically with shoulder diameter. The X-axis force registered a relatively steep increase up to a shoulder diameter of 18 mm; beyond this shoulder diameter, the variation in X-axis force is negligible. As indicated above, (Fig. 7) the heat input increases with shoulder diameter. An increasing heat input produces a large volume of plasticized material around the pin, which in turn induces a relatively higher force on the pin. This duly explains the increase in x-axis force with higher heat input, while employing a larger shoulder diameter. An increasing vertical downward force (Z-axis force) and spindle torque with increasing shoulder diameter is due to the larger shoulder/metal contact area during welding as shown in Fig. 9.

3.3 Shoulder Driven Metal Flow

At a given rotational speed and travel speed, the volume of shoulder driven metal-flow reduces with increasing

shoulder in the radially outward direction is shown in Table 3. It may be observed that this temperature gradient becomes less steep with increasing shoulder diameter, reaching a minimum for the 18 mm diameter shoulder.

Table 3 Spatial temperature gradient under the different shoulders

Sl. no.	Shoulder radius S_r (mm)	Pin radius P_r (mm)	T_{max} °C at pin peripheral	T_{mid} °C at shoulder mid radius	T_{min} °C at shoulder peripheral	ΔT °C ($T_{max} - T_{min}$)	Distance $S_r - P_r = d$ (mm)	$\Delta T/d$
1	5.75	3	288	262	178	110	2.75	40.00
2	6	3	291	268	180	111	3.0	37.00
3	7.5	3	392	338	220	172	4.5	38.22
4	9	3	405	352	228	177	6.0	29.50
5	11.5	3	420	383	240	180	7.5	24.00
6	12	3	453	395	245	208	9.0	23.11

Fig. 7 Variation of heat input with different shoulder diameters

Fig. 8 Force and torque profiles for weld produced with 12 mm shoulder diameter
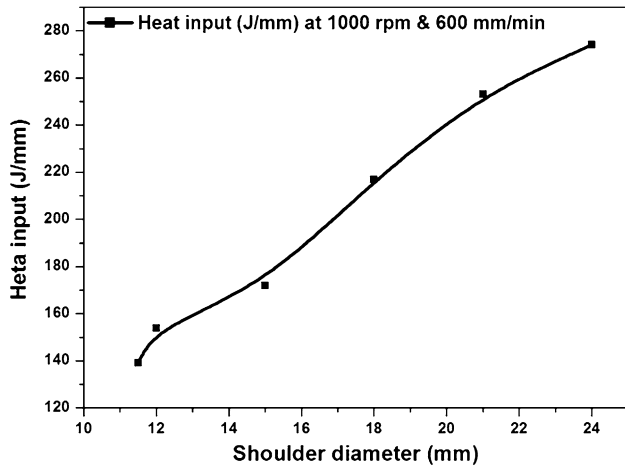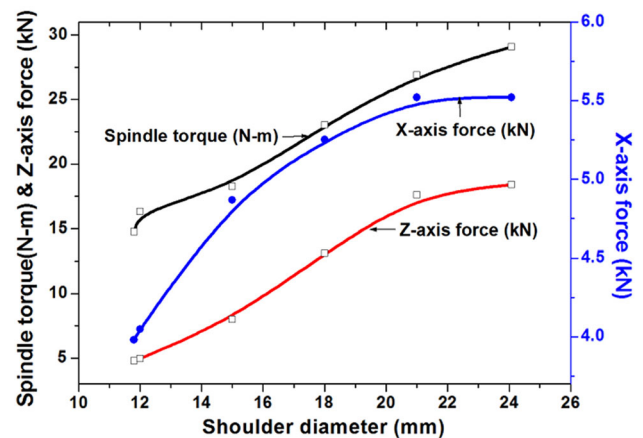

Fig. 9 Variation of force and torque acting on pin with respect to change in shoulder diameter

shoulder diameter (Fig. 10). It may be recalled that the annular area, responsible for a major part of frictional heat generation by the shoulder, gets saturated with the increase in shoulder diameter (Table 2). Since the measured peak temperatures registered a monotonic increase with shoulder diameter, it follows that the temperature difference increases between the workpiece and tool as well as the shoulder driven flow area and surrounding material. This steeper temperature gradient, coupled with a larger area of contact (with increase in shoulder diameter) results in higher heat losses through conduction to the surrounding material as well as to the tool. Thus, although the heat-input increases considerably with shoulder diameter, the heat losses are also greater. Hence, the volume of shoulder driven material flow registers a marginal decrease with an increase in shoulder diameter, owing to a relatively smaller volume of material plasticized by the available heat. This argument is also reinforced by the larger torque values recorded at higher shoulder diameters. That is, a higher frictional resistance has to be overcome by the larger diameter shoulder, due to larger contact area as well as relatively lesser plasticized region underneath. From Fig. 10, it may be observed that there is a monotonic increase in the TMAZ with increase in shoulder diameter. This is also presented in Table 4. Although TMAZ
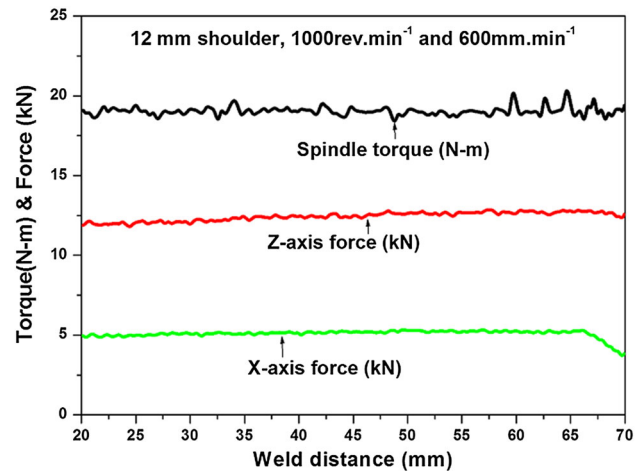
underwent plastic deformation, recrystallization did not occur in this zone due to insufficient plastic strain and heat-input. The stir zone (SZ) exhibited fine and equiaxed grain structure with an average grain diameter of 2.6 μm and typical microstructure (EBSD) of friction stir weld produced by 12 mm shoulder is shown in Fig. 11. The average
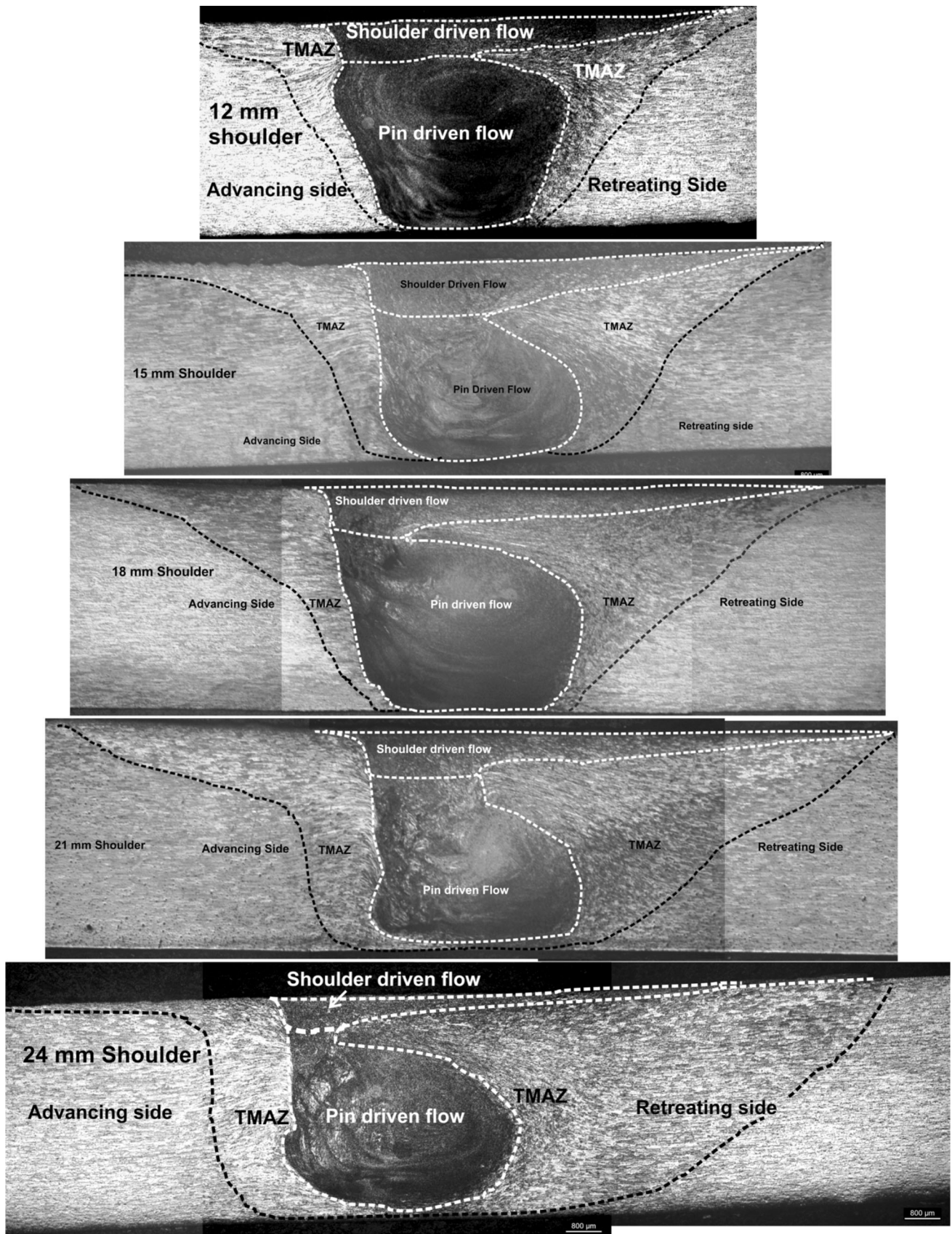
Fig. 10 Area of shoulder driven material flow and TMAZ width at constant rotational speed and traverse speed for different shoulder diameters

Table 4 Area of pin/shoulder driven material flow and TMAZ width with different shoulder diameters

Shoulder diameter (mm)	Pin driven/shoulder driven material flow area (mm^2)		TMAZ width (mm)	
	Pin driven flow	Shoulder driven flow	Advancing side	Retreating side
12	17.67	6.21	0.41	1.19
15	17.22	6.09	1.14	3.04
18	14.46	5.97	1.26	3.13
21	13.98	5.78	1.46	3.62
24	15.08	5.38	1.90	6.38

Fig. 11 Typical stir zone microstructure (EBSD) of friction stir weld produced by 12 mm shoulder
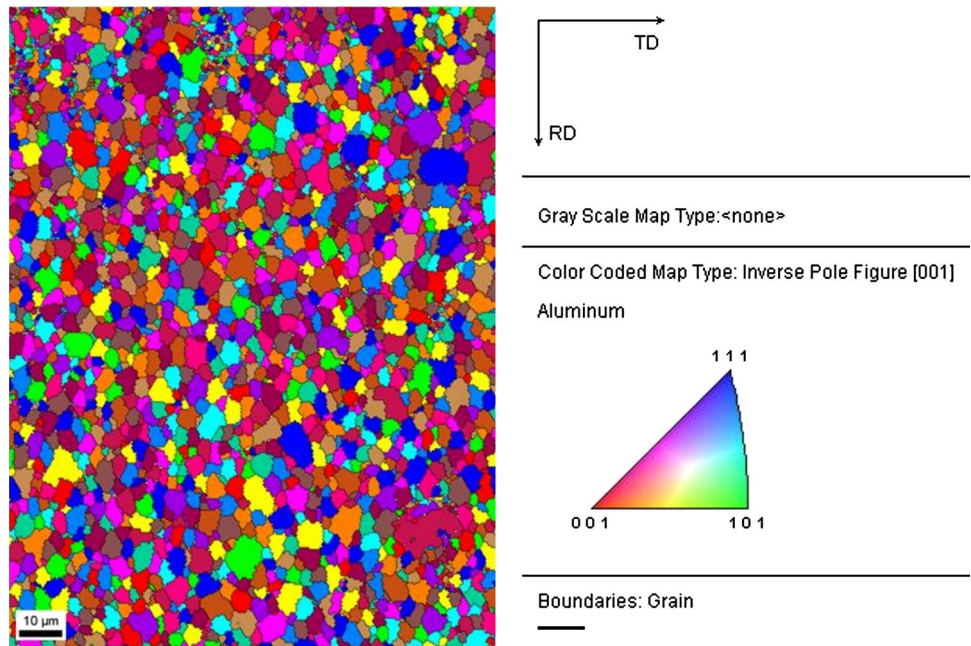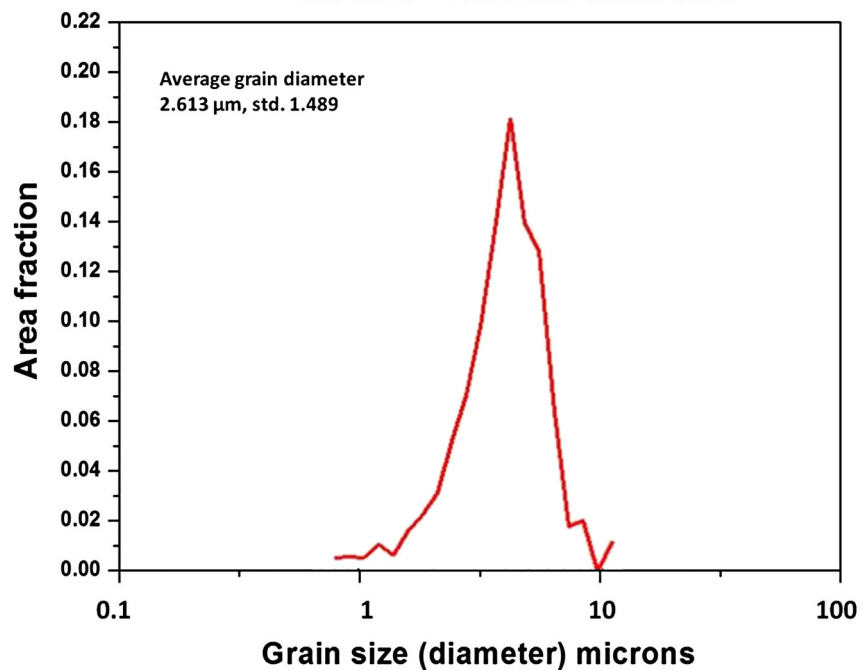
grain size of the stir zones of the welds fabricated by different shoulder diameters is presented in Table 5.

3.4 Zener–Hollomon Parameter (Z)

In FSW process, the quality of the joints is critically dependent on the plasticity of material at hot forming temperatures. The strain-rates encountered in the process are very high, of the order of $10^3 s^{-1}$. The high temperature flow-stress of the material, which in turn is a function of the Zener–Hollomon Parameter 'Z (temperature compensated strain-rate), determines the all important plasticity of the material under the combined effect of temperature and strain-rate. In other words, the value of 'Z' at any location in the FSW region may be considered as the index of flowability of the material, with a direct influence on the soundness of the joint. The variation of 'Z' with radial distance, between the periphery of the pin to the periphery of the shoulder is presented in Fig. 12. The peak temperature at the nugget–TMAZ boundary (close to the plate surface below the shoulder) increases with the shoulder diameter (Fig. 6). The predominant effect of temperature on the flow-stress is represented by the variation of 'Z' at 3 mm radial distance from the rotating tool axis (pin periphery) for different shoulder diameters; that is, 'Z' decreases continuously with an increasing shoulder diameter at the pin periphery. Since strain-rate is equal at the pin periphery for all tools (due to the equal tool rotational speed employed in all cases), the variation in 'Z' (and consequent variation in flow-stress) is essentially attributed to the temperature.

The variation of 'Z' with radial distance for tools of different shoulder diameters represents the variation of flow-stress at different points in the radially outward direction. It may be observed that for smaller shoulder diameter (12 mm), the 'Z' (and hence flow-stress) increases steeply in the radial direction towards the shoulder periphery. With increasing shoulder diameter from 15 to 21 mm, 'Z' reaches a comparable peak value but gradually. This trend indicates that plasticity is confined to the immediate vicinity of the pin in the case of 12 mm shoulder diameter. That is, due to the steep increase in flow-stress, the plasticity reduces sharply in the radially outward direction. The tools with gradually increasing 'Z' signify plasticity over a relatively larger region around the pin. However, the periphery of the shoulder indicates negligible plasticity due to high 'Z'. In the case of 24 mm shoulder diameter, the rate of increase of 'Z' with radial distance is very low. The relatively lower 'Z' at corresponding radial locations in the case of 24 mm shoulder points to a somewhat lower flow-stress, which in turn results in some level of plasticity (although subdued) all over the region below the shoulder. This phenomenon is

Table 5 The average grain size in the stir zones produced by different shoulder diameters

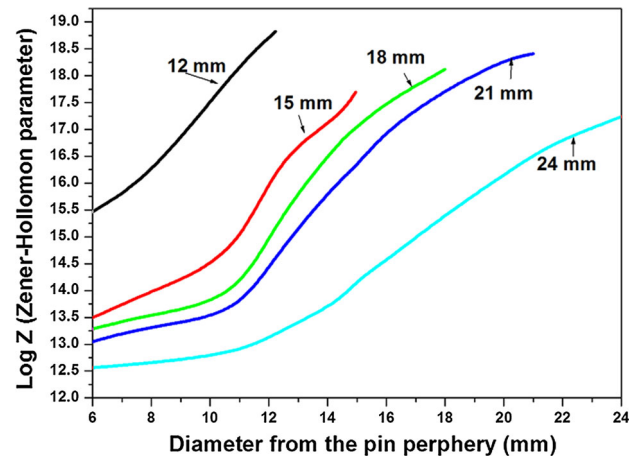| Sl. no.	Shoulder diameter (mm)	Average grain diameter (μm) in stir zone
1	12	2.61
2	15	2.72
3	18	2.75
4	21	2.80
5	24	2.82

Fig. 12 Variation of 'Z' along the radial distance (pin periphery to the shoulder periphery)

Table 6 Hot working range of temperature and strain-rate as per the process map [42]

Sl. no.	Condition	Temperature range °C (K)	Strain rate (s⁻¹)	Z parameter (s⁻¹)	Log Z
1	Dynamic recrystallization	380 (653)	10	3.94×10^{12}	12.595
		500 (773)	10^{-3}	6.27×10^{6}	6.797
2	Dynamic recovery	340 (613)	100	2.26×10^{14}	14.354
		420 (693)	3	2.53×10^{11}	11.4
3	Flow instability	330 (603)	>1	3.62×10^{12}	12.595
4	Weld nugget	487 (760)	107.43	9.93×10^{11}	11.99

brought about by a large rotating layer characterized by distorted grains (due to low-working temperature, probably in the warm working regime) below the tool shoulder in the case of 24 mm. Additionally, the relatively high amount of digging-in by larger diameter shoulders, due to the tool tilt, may also be contributing to a wider TMAZ below the shoulder.

Hot plastic deformation of AA 2014 has also been interpreted in light of the processing maps, developed for a similar alloy AA 2024 [42]. According to the processing
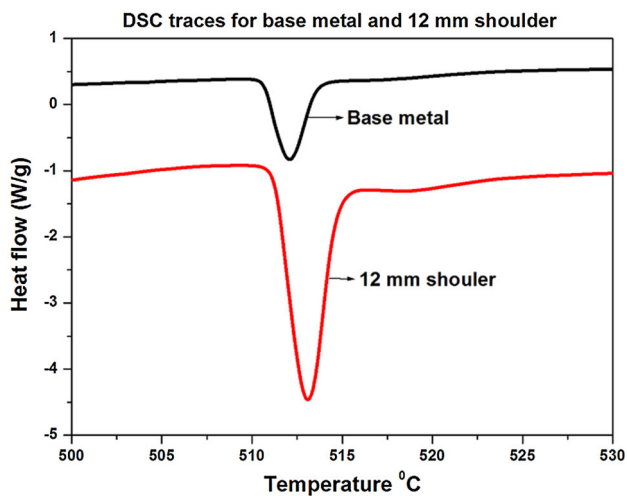
Fig. 13 Differential scanning calorimetry (DSC) curves for stir zone and base metal

map, the alloy undergoes dynamic recrystallization in the temperature range of 380–500 °C and strain-rate range 10^{-3} to 10 s^{-1}. It is also observed that dynamic recovery occurs in the temperature range of 340–420 °C at strain-rates 3–100 s^{-1}; flow instability is reported at temperatures less than 330 °C and strain-rates above 1 s^{-1}. This data has been converted into equivalent ranges of 'Z' parameter as shown in the Table 6.

The temperature and strain-rate in the nugget region of FSW is influenced by the rotational speed and travel speed apart from the pin geometry [31]. Since the pin geometry, rotational speed and travel speed are equal, the nugget region may be expected to be identical in the welds produced by different shoulder diameters. Estimated temperature and strain-rate for the nugget region are 487 °C and 107.43 s^{-1}, respectively. 'Z' evaluated for the nugget region is 9.93×10^{11}, as may be observed from the Table 6. The 'Z' for nugget region falls in the dynamic recrystallisation region for the material, thereby ensuring a fine and equiaxed grain structure as shown in EBSD image, Fig. 11. Metallographic analysis of the nugget material validated these observations. DSC traces for the weld and base metal are shown in Fig. 13. The graph clearly reveals

that the endothermic peaks are obtained at temperatures between 512 and 514 °C, which corresponds to a complete dissolution of precipitates as may be observed from the phase diagram. The deformation and weld quality in the TMAZ and stirred region were also analyzed with the Zener–Hollomon parameter, evaluated using the experimentally measured temperatures and estimated strain-rates. The variation of estimated 'Z' values for various shoulder diameters is presented in Table 7. In general, a higher 'Z' resulted in relatively larger TMAZ region.

4 Summary

In this investigation, the influence of shoulder diameter on weld performance is evaluated. Of the six joints fabricated using tools with different shoulder diameters at 1,000 rpm and 600 mm/min, the weld bead appearance is smooth without any surface defects in the welds produced with shoulder diameters from 12 to 15 mm. With a further increase in the shoulder diameter from 18 to 24 mm, surface defects were noticed. Peak temperatures measured below the shoulder, at the Nugget/TMAZ interface; increase with an increasing shoulder diameter. The temperature gradient also becomes less steep with increasing shoulder diameter, reaching a minimum for the 18 mm diameter shoulder. Beyond this, there is a moderate decrease in the temperature gradient up to 24 mm shoulder diameter. At a given rotational speed, the volume of shoulder driven metal-flow reduces, although marginally with increasing shoulder diameter.

The investigation brings out an important conclusion that the shoulder diameter does not contribute to the quality of FSW, because of the saturation in the frictional heat generating annular area. The well documented processing maps for different materials provide a valuable insight into the plastic deformation behaviour, which in turn is useful in optimizing the FSW tool geometry and process parameters to obtain defect free welds. The processing maps have been effectively utilized to develop a systematic understanding of the FSW process from a metal working

Table 7 Variation of strain rate, temperature and Z parameter with shoulder diameter

Shoulder diameter (mm)	Periphery of the pin			Middle of the shoulder			Periphery of the shoulder		
	Strain rate (s^{-1})	Temp. °C	Log Z	Strain rate (s^{-1})	Temp. °C	Log Z	Strain rate (s^{-1})	Temp. °C	Log Z
11.5	123.86	288	15.59	133.18	262	16.28	136.58	178	18.92
12	124.46	290	15.52	134.25	268	16.12	138.00	180	18.85
15	127.87	392	13.49	140.00	338	14.54	145.44	220	17.52
18	130.14	405	13.28	144.94	352	14.27	151.51	228	17.29
21	133.14	420	13.04	149.21	383	13.71	156.66	240	16.95
24	135.17	453	12.56	152.99	395	13.52	161.05	245	16.83

perspective for the first time. The Zener–Hollomon parameter can be used to develop a scientific understanding of the formation of defects in FSW, due to an in-appropriate plastic deformation behaviour in the stir region and in its vicinity.

References

1. Threadgill P L, Leonard A J, Shercliff H R, and Withers P J, *Int Mater Rev* **54** (2009) 49.
2. Sindo K, *Welding Metallurgy*, 2nd edn, John Wiley & Sons, Inc., Publication, New York (2003).
3. Nandan R, DebRoy T, and Bhadeshia H K D H, *Prog Mater Sci* **53** (2008) 980.
4. Mishra R S, and Ma Z Y, *Mater Sci Eng R* **50** (2005) 1.
5. Bhadeshia H K D H, and DebRoy T, *Sci Technol Weld Join* **14** (2009) 193.
6. Ramanjaneyulu K, Madhusudhan Reddy G, Venugopal Rao A, and Markandeya R. *J Mater Eng Perform* (2013). doi: 10.1007/s11665-013-0512-4.
7. Rajakumar S, and Balasubramanian V, *J Mater Des* **34** (2012) 242.
8. Chen Y C, and Nakata K, *J Mater Des* **30** (2009) 3913.
9. Bilici M K, and Yükler A I, *J Mater Des* **33** (2012) 145.
10. Khodaverdizadeh H, Heidarzadeh A, and Saeid T, *J Mater Des* **45** (2013) 265.
11. Elangovan K, and Balasubramanian V, *J Mater Des* **29** (2008) 362.
12. Kumar K, and Kailas S V, *Mater Sci Eng A* **485** (2008) 367.
13. Rajakumar S, Muralidharan C, and Balasubramanian V, *J Mater Des* **32** (2011) 535.
14. Leal R M, Leitao C, Loureiro A, Rodrigues D M, and Vilac P, *Mater Sci Eng A* **498** (2008) 384.
15. Malarvizhi S, and Balasubramanian V, *J Mater Des* **40** (2012) 453.
16. Yasunari T, Yoshihiko U, and Keiro T, *Int J Mach Tools Manuf* **47** (2007) 2230.
17. Liu F C, Ma Z Y, and Chen L Q, *Scr Mater* **60** (2009) 968.
18. Arora A, De A, and Deb Roy T, *Scr Mater* **64** (2011) 9.
19. Akinlabi E T, *J Mater Eng Perform* **21** (2012) 1514.
20. Scialpi A, De Filippis L A C, and Cavaliere P, *J Mater Des* **28** (2007) 1124.
21. Mehta M, Arora A, De A, and Debroy T, *Metall Trans A* **42A** (2011) 2716.
22. Zhang Z, Liu Y L, and Chen J T, *Int J Adv Manuf Technol* **45** (2009) 889.
23. Titilayo E A, *Adv Mater Res* **299–300** (2011) 1146.
24. Schmidt H N B, Dickerson T L, and Hattel J H, *Acta Mater* **54** (2006)1199.
25. Zhao Y H, Lin S B, Qu F X, and Wu L, *Mater Sci Technol* **22** (2006) 45.
26. Guerra M, Schmidt C, McClure J C, Murr L E, and Nunes A C, *Mater Charact* **49** (2002) 95.
27. Chen Z W, Pasang T, and Qi Y, *Mater Sci Eng A* **474** (2008) 312.
28. Chen ZW, and Cui S, *Scr Mater* **58** (2008) 417.
29. Fratini L, Buffa G, Palmeri D, Hua J, and Shivpuri R, *Sci Technol Weld Join* **11** (2006) 412.
30. Seidel T U, and Reynolds A P, *Metall Mater Trans A* **32** (2001) 2879.
31. Arbegast W J, *Modeling Friction Stir Joining as a Metalworking Process, Hot Deformation of Aluminum Alloys III*, ed. Z. Jin, TMS (The Minerals, Metals, and Materials Society), Warrendale (2003).
32. Nilesh K, and Mishra Rajiv S, *Metall Mater Trans A* **44A** (2013) 934.
33. Nandan R, Roy G G, Lienert T J, and Debroy T, *Acta Mater* **55** (2007) 883.
34. Ghosh M, Kumar K, and Mishra R S, *Scr Mater* **63** (2010) 851.
35. Reynolds A P, *Scr Mater* **58** (2008) 338.
36. Long T, Tang W, and Reynolds AP, *Sci Technol Weld Join* **12** (2007) 311.
37. Arbegast W J, and Hartley P J, in Proceedings of the 5th International Conference on Trends in Welding Research, Pine Mountain (1998) 541.
38. Cerri E, and Leo P, *J Mater Des* **31** (2010) 1392.
39. Lammlein D H, De Lapp D R, Fleming P A, Strauss A M, and Cook G E, *J Mater Des* **30** (2009) 4012.
40. Leitao C, Louro R, and Rodrigues D M, *J Mater Des* **37** (2012) 402.
41. Forcellese A, and Simoncini M, *J Mater Des* **36** (2012) 123.
42. Prasad Y V R K, and Sasidhara S. *Hot Working Guide: A Compendium of Processing Maps*, ASM International (1997).